Wiley
International Journal of Energy Research
Volume 2024, Article ID 6788210, 19 pages
https://doi.org/10.1155/2024/6788210

WILEY

*Research Article*

# Hybrid Heat Pipe Shutdown Rod as a Novel Concept of Passive Safety System for Microreactor

**Dong Hun Lee and In Cheol Bang**

*Department of Nuclear Engineering, Ulsan National Institute of Science and Technology (UNIST), 50 UNIST-gil, Ulju-gun, Ulsan 44919, Republic of Korea*

Correspondence should be addressed to In Cheol Bang; icbang@unist.ac.kr

Received 7 November 2023; Revised 14 March 2024; Accepted 22 May 2024

Academic Editor: Sunday Olayinka Oyedepo



Ensuring the structural integrity of the monolithic core, which houses critical components such as heat pipes and fuel rods, is crucial for the safety of a microreactor. This research introduces a hybrid heat pipe shutdown rod as a novel passive safety system to address potential temperature rises in the monolithic core during accidents. It is designed to perform a dual function under accident conditions. It simultaneously absorbs neutrons and removes heat through structural modifications to the existing shutdown rod. Specifically, this system provides a heat transfer path within the monolithic core without increasing the size of the microreactor. By selecting cesium as the working fluid, we aimed to achieve rapid operation of the heat pipe to quickly reduce the temperature gradient in the monolithic core under accident conditions. The hybrid heat pipe was fabricated and evaluated and found to develop continuous flow even at temperatures around 205.1°C. However, its unique structure causes a pronounced converging–diverging effect, resulting in a temperature drop from about 70–170°C in the evaporator region, followed by a slight recovery to below 50°C in the condenser. This effect arises from changes in the cesium vapor mass flow rate due to phase changes and variations in the flow area between the evaporator and condenser. Despite these effects, the use of liquid cesium as the working fluid enables the hybrid heat pipe to operate under natural convection, avoiding startup problems that could cause flow blockage.

## 1. Introduction

As the nuclear industry places increasing emphasis on passive safety and mobile energy sources, there is growing interest in microreactors that can use passive heat transfer mechanisms for indefinite cooling. Microreactors typically generate power in the range of a few kilowatts to 20 MW. These reactors often use heat pipes to transfer heat from the core to a heat exchanger or power conversion system, called heat pipe-cooled reactors (HPRs). Heat pipes are highly efficient heat transfer devices that can transfer heat over long distances using a two-phase process. HPRs generally operate at high temperatures, typically between 500 and 800°C, and their main components include liquid metal heat pipes, which are known for their excellent heat transfer performance and passive operation. They play a critical role as the primary heat transfer system in microreactors. As summarized in Table 1, the designs currently proposed for microreactors vary according to their intended use.

A typical HPR consists of liquid metal heat pipes, control drums, shutdown rods, and a monolithic core supporting these components. A prime example of this type of reactor is the Westinghouse eVinci design shown in Figure 1. Fuel rods and heat pipes are typically inserted into the holes in the monolithic core, while control drums are used for reactivity control. Several monolithic core designs are under consideration. One approach uses graphite as the material for the monolithic core block. This block houses both the heat pipes and the fuel and acts as a moderator. An alternative strategy separates the functions of the solid core block, which could be made of graphite or stainless steel, from that of the moderator. In this design, materials such as $YH_x$ are used as moderator rods and inserted into the monolithic core. The liquid metal heat pipes, which are ~4 m in length, utilize a wick structure within their cladding to facilitate liquid

Table 1: Currently proposed designs of heat pipe-cooled microreactor.

| Reference | Heat pipe information | | | Microreactor design | | |
|---|---|---|---|---|---|---|
| | Container | Wick | Working fluid | Fuel type | Reactivity control | Purpose (operating condition) |
| Kilopower [1] | Haynes-230<br>$H = 1.3$ m (0.35 : 0.86 : 0.09)<br>$D = 12.7$ mm | Artery wick | Na | UMO | Control rod shutdown rod | Space (microgravity) |
| Megapower [2] | Stainless steel<br>$H = 4.0$ m (1.5 : 0 : 2.5)<br>$D = 15.75$ mm | N/A | K | $UO_2$ | Control drum shutdown rod | Transportable (horizontal) |
| eVinci [3] | FeCrAl<br>$H = 4.0$ m (N/A)<br>$D =$ N/A | Tubular wick | Na | TRISO (HALEU) | Control drum shutdown rod | Transportable (horizontal) |
| Aurora [4] | Stainless steel<br>$H =$ N/A<br>$D =$ N/A | Porous wick | K | U-10Zr | Control rod shutdown rod | Stationary (vertical) |
| INL design [5] | Stainless steel<br>$H = 4.0$ m (1.5 : 0.4 : 2.1)<br>$D = 18$ mm | Screen wick | K | $UO_2$ | Control drum shutdown rod | Transportable (horizontal) |

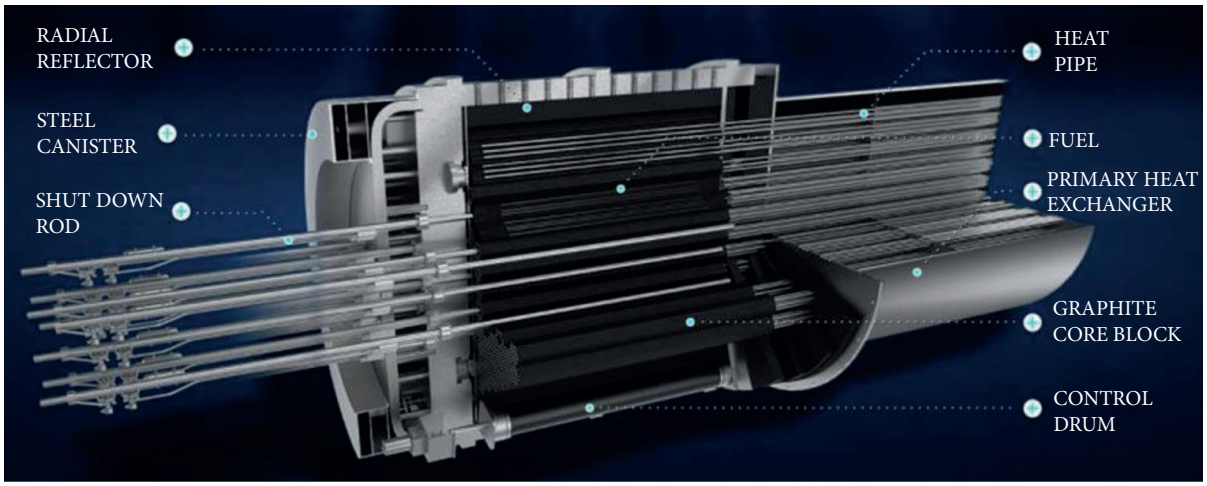


Figure 1: Configuration of representative monolith core type microreactor (eVinci, Westinghouse) [6].

transport under horizontal operating conditions. The evaporator section of the heat pipe is aligned with the height of the fuel rod inserted into the monolithic core, where the heat vaporizes the working fluid. This vapor, which carries a significant amount of latent heat, is then directed to the condenser, where it condenses. The condensed liquid is returned to the evaporator by gravity or capillary action. This ensures continuous circulation even in horizontal or microgravity conditions. With hundreds to thousands of heat pipes integrated into the monolithic core, the independent and passive operation of each heat pipe not only enhances the system's overall safety but also improves reactor redundancy. This design effectively mitigates the risk of failure of a single heat pipe, ensuring uninterrupted operation of the entire system.

In microreactors, maintaining the structural integrity of the monolithic core is one of the safety objectives. This core serves as the fundamental structure for housing both the heat-generating fuel rods and the heat-dissipating heat pipes. Therefore, it is critical to ensure the structural integrity of the core to prevent the energy balance of the microreactor. Specially, the monolithic core must remain undamaged and free of cracks or fractures. Currently, various materials are considered for the monolithic core. Stainless steel is often the preferred choice due to its exceptional manufacturability, compatibility, and its role in achieving negative reactivity

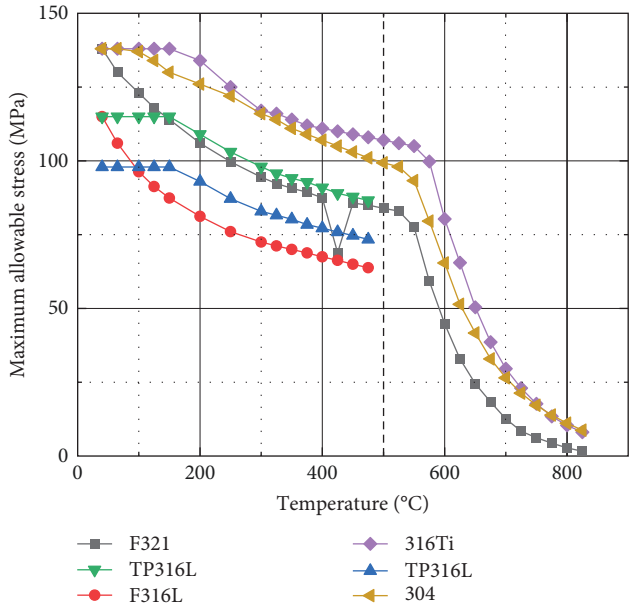


FIGURE 2: General maximum allowable stress behavior of typical stainless steels according to ASME material code.

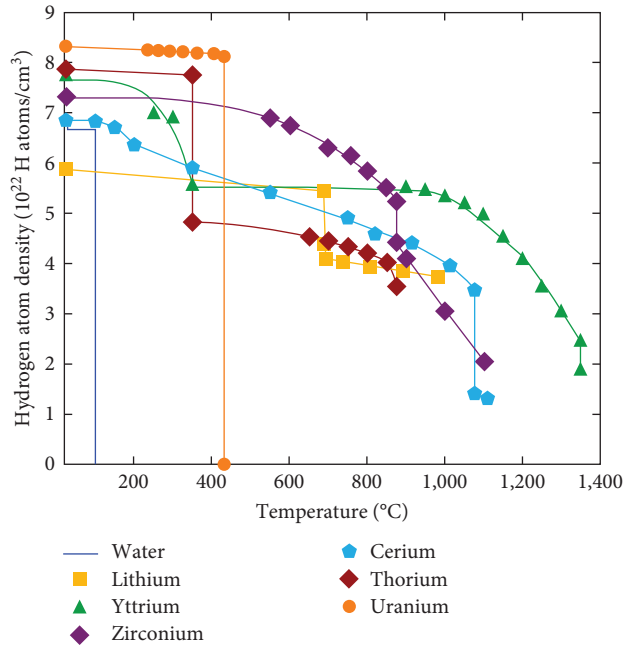


FIGURE 3: General behavior of hydrogen retention with temperature [10].

feedback in reactor design. Negative reactivity feedback refers to increased neutron leakage resulting from thermal expansion of the monolithic core at elevated temperatures. However, it is important to consider factors such as thermal creep, fatigue, and temperature gradients. These factors become more pronounced at higher temperatures. Figure 2 shows the allowable stress values for stainless steel according to the ASME material standards and shows that there is a significant decrease at above 500°C. At 800°C, the allowable maximum stress is approximately one-fifth of that at 500°C. This underscores the importance of managing the temperature of the monolithic core to maintain its structural integrity. Graphite is considered a leading candidate material for the monolithic core in the eVinci microreactor design [3]. The extensive use of graphite as a moderator in nuclear reactors underscores the need to maintain mechanical stability in irradiated environments, especially by avoiding significant temperature increases. Both radiation dose and temperature affect graphite degradation. More significant reductions in the life of graphite moderators are observed at elevated temperatures [7]. Therefore, attention to operating temperature is critical to use graphite as a microreactor core material. Recent studies have also explored the possibility of the use of composite moderators such as $YH_x$ in advanced microreactors that operate at higher temperatures and have more compact core designs [8]. However, a potential issue with employing $YH_x$ as a moderator is the redistribution of hydrogen within the core under thermal gradients [9]. As shown in Figure 3, the hydrogen atom density in yttrium exhibits two distinct regions of rapid decrease with increasing temperature, indicating that temperature gradients can cause hydrogen emission within the microreactor. Therefore, minimizing the temperature gradient in the monolithic core is critical to ensure its mechanical stability under any core configuration.

Various studies have been conducted to investigate the structural safety of monolithic cores, encompassing advanced manufacturing, sensing, structural optimization, and the numerical analysis of thermal stress. In order to evaluate the structural integrity under both normal operation and accident conditions, some studies have performed thermal-mechanical safety analysis. Qin et al. [11] used STAR-CCM+ to simulate a monolithic core with a single heat pipe inserted and evaluate the stress distribution. They observed that the maximum stress was in the line connecting the center of each hole, and significant thermal stress was found in the shortest path between the heater and the heat pipe. Jeong [12] and Jeong et al. [13] conducted stress analysis on the monolithic core using OpenFOAM coupled with the ANL/HTP code, which is commonly employed for heat pipe thermal evaluation. They highlighted the significant influence of temperature distribution on thermal stress and emphasized the importance of flattening the temperature profile in the core to meet the stress limits specified in the ASME Code. Hyer et al. [14] focused on sensing technology, specifically on the installation of embedded sensors using ultrasonic additive manufacturing to monitor the structural health of the monolith. Similarly, Birri et al. [15] explored the use of fiber optic and acoustic sensors on the monolithic core for detecting structural defects. Currently, these advanced sensing technologies are limited to low temperatures and simple structures. However, they have the potential to be applied to the monitoring and management of strain and thermal stress in the monolithic core of a microreactor.

To maintain the structural safety of the monolithic core, it is essential to prevent large temperature gradients. Previous simulation research has shown that even if a few liquid metal heat pipes fail, adjacent heat pipes can absorb the excess heat and prevent large temperature gradients within the monolithic core [16, 17]. However, this safety margin is only guaranteed if the evaporator and condenser sections of

the heat pipes function normally. A critical factor to consider is that all the heat pipes inserted into the monolithic core utilize the same heat exchanger as the condenser. The heat transfer performance of the liquid metal heat pipes may be adversely affected in the event of an accident where the heat exchanger loses or degrades its cooling capacity, and an unexpected rapid increase in the temperature of the monolithic core could occur in this situation. This concern, related to accident scenarios for microreactors, has been discussed in the Phenomena Identification and Ranking Table by INL [2], and Antonello et al. [18] conducted a safety analysis of microreactor and also noted that the most critical scenarios are associated with the occurrence of a loss of heat sink. If the flow within the heat exchanger becomes fully or partially blocked, alternatives to serve as a cooling are needed. However, since the heat pipes are embedded within the heat exchanger, bypassing may not be a feasible option. The shutdown rod automatically performs a passive function to shut down the reactor. In microreactors, however, there is no safety cooling system within the core to remove heat. Decay heat is removed only by conduction and radiation from the solid structure to the ambient air. As a result, the temperature gradients resulting from the degradation of the heat pipe performance may increase the risk of cracking or fracture of the monolithic core. In this study, a novel concept of a passive safety system that can be implemented within microreactors is proposed to address these concerns. The design purpose of this proposed safety system is as follows:

(1) Minimizing the increase in the size of microreactors is a significant advantage. This is due to their special purpose for transportation and ease of installation, making them suitable for various applications.
(2) The proposed safety system is designed to operate passively to minimize its size. It should not rely on any electrical or mechanical components.
(3) It is designed to flatten temperature distribution within a solid core, even if a heat exchanger failure occurs, which affects all heat pipe condensers in a solid core. This measure is necessary to prevent the monolithic core-to-temperature gradients caused by heat pipe performance degradation.

To achieve the design objectives mentioned above, this paper introduces a novel concept of a passive safety system for microreactors. The proposed concept aims to perform a hybrid function during accident conditions by simultaneously absorbing neutrons and removing heat through structural modifications to the existing shutdown rod. The characteristics of the proposed hybrid heat pipe shutdown rod are as follows:

(1) The hybrid heat pipe shutdown rod has been proposed as a potential passive safety system for microreactors. It is capable of performing both neutron absorption and heat removal functions by incorporating structural modifications into the shutdown rod. This system offers the advantage of not requiring an increase in the size of the microreactor, as shutdown rods are already an integral part of the microreactor design.
(2) Heat pipes operate passively by capillary force, making them well-suited for use in passive safety systems. In addition, the use of air as the ultimate heat sink allows the hybrid heat pipe shutdown rod to operate even in the event of a heat exchanger failure. To achieve this, the shutdown rods are installed in a configuration opposite to the heat pipe connected to the heat exchanger.
(3) Liquid cesium, which is suitable for medium-temperature heat pipes due to its relatively high vapor pressure, is used as the working fluid of the hybrid heat pipe shutdown rod. Compared to other liquid metals such as sodium and potassium, choosing liquid cesium as the working fluid allows the heat pipe to operate even at low temperatures.

UNIST has previously proposed a hybrid heat pipe control rod concept for emergency core cooling systems in pressurized water reactors (PWRs) [19], as well as an additional heat transfer path for dry storage casks [20, 21]. Various experiments and simulations have been conducted to verify its performance. However, there are significant differences between the hybrid heat pipe safety system concept for microreactors and that for conventional nuclear reactors, particularly with respect to the dimensions and shapes. First, due to the use of fuel assemblies in conventional reactors, the size and shape of the control rods must take into account the size of the grid. As a result, the outer diameter of the hybrid heat pipe cladding is typically less than 0.5 inch. The rods have a large $L/D$ (length to diameter) ratio due to their long length. In contrast, the design of the shutdown rods of the hybrid heat pipe for microreactors can be modified according to the hole size of the monolithic core, which allows for more flexibility. Since the heat transfer performance of a heat pipe is greatly affected by the diameter of the heat pipe, this design flexibility allows heat pipes with higher heat removal performance. In addition, the configuration of microreactors provides flexibility in the design of hybrid heatpipe shutdown rods. The shutdown rod can be designed with different dimensions and shapes without the constraint of being assembled with the control rod, since the control drum can replace the role of the control rod in PWRs. This allows for more custom and optimized designs for specific microreactor applications, which is not possible with conventional reactors. For example, Alawneh et al. [22] proposed a design of a heat pipe-cooled microreactor with a square-shaped solid core consisting of four monolithic cores with a power level of 3 MW. A control drum for reactivity control and a shutdown rod for passive shutdown were installed in the microreactor. The shutdown rod had a cross-shaped design, demonstrating that the design of shutdown rods in microreactors can be more flexible. Similarly, the Holos-Quad microreactor [23] also had a cross-arranged shutdown rod. This demonstrates the potential for different shapes and arrangements of shutdown rods in microreactors compared to those in PWRs. Second, depending on the application, microreactors operate in a variety of conditions. These

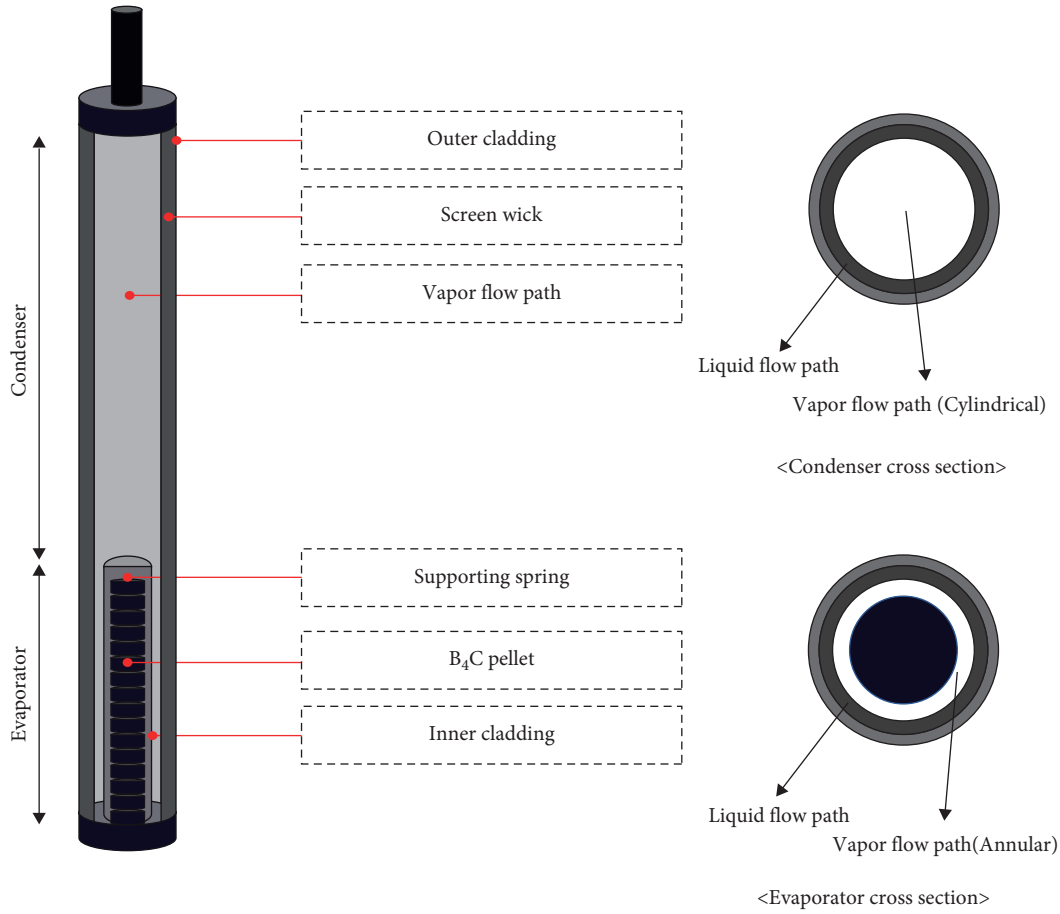


FIGURE 4: Schematic configuration of hybrid heat pipe shutdown rod.

include vertical, horizontal, and microgravity. Therefore, the dependence on capillary force is more critical compared to the application in light water reactors, which mainly operate in vertical conditions. Finally, since microreactors use liquid metal heat pipes to operate at high temperatures, a working fluid other than water should be used in the shutdown rod to avoid chemical reactions.

Since this is a new concept for microreactors, with distinct differences from previously proposed hybrid heat pipe concepts, the aim of this paper is to verify the concept through the fabrication and experimentation of a hybrid cesium heat pipe shutdown rod proposed as a passive safety system for microreactors. In Section 2, the characteristics of the proposed hybrid heat pipe are summarized, while in Section 3, the fabrication process and the experimental setup for the heat pipes are described. The analysis and discussion of the results are reported in Section 4. This research will be a contribution to the development of safer, smaller, and more innovative designs for microreactors.

## 2. Design of Hybrid Shutdown Rod

*2.1. Concept of Hybrid Heat Pipe Shutdown Rod.* The hybrid heat pipe for microreactors represents an innovative concept in passive decay heat removal systems. It integrates the functions of both a shutdown rod and a heat pipe. Figure 4 shows the configuration of the hybrid heat pipe. It has an inner cladding with $B_4C$ neutron absorbers. The outer cladding consists of wick structures with a working fluid for passive heat transfer. The area of the vapor flow path greatly affects the heat transfer performance of a heat pipe. The inner cladding containing the $B_4C$ absorber was strategically placed only in the evaporator section of the heat pipe to minimize the adverse effect on heat transfer performance of reducing the vapor flow area. Consequently, the vapor generated flows along an annular path in the evaporator section and then transitions to cylindrical in the condenser section.

A schematic of hybrid heat pipe designs suitable for integration into microreactors is shown in Figure 5. Hybrid heat pipes can provide an additional heat transfer path within the microreactor during accident scenarios, because designed to automatically insert into the monolithic core. This safety system effectively mitigates the temperature rise in the monolithic core by using phase-change heat transfer in conjunction with conventional conduction and radiation in solid structures and prevents the adverse effects of decay heat. In addition, the safety of microreactors can be enhanced without the need for additional systems, as hybrid heat pipes can replace conventional shutdown rods. To optimize this advantage, the heat sink of the hybrid heat pipe is designed to use environmental air cooling under all operating conditions of

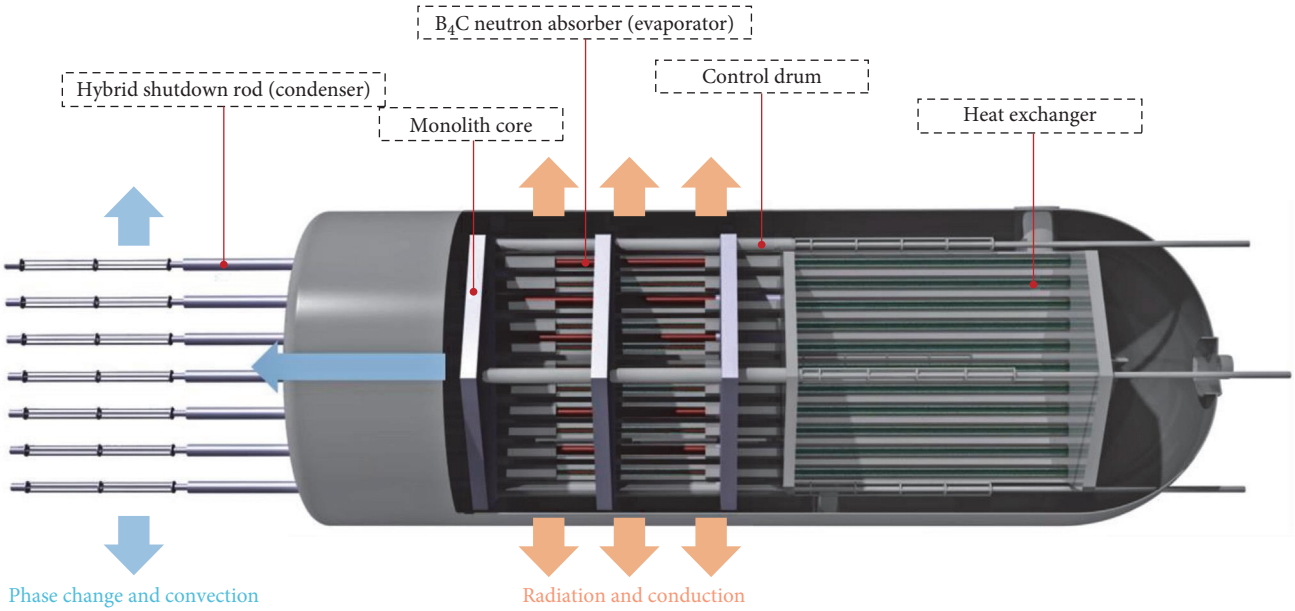


FIGURE 5: Schematic diagram of a hybrid heat pipe for microreactor applications.

the microreactor. Unlike PWRs, where the control and shutdown rods are assembled as a single unit, microreactors have separate shutdown rods and control drums. This arrangement minimizes heat loss through the hybrid heat pipe under normal operating conditions, since the shutdown rod is only inserted under unexpected circumstances.

*2.2. Working Fluid of Hybrid Heat Pipe Shutdown Rod.* The proper selection of a suitable working fluid is crucial for the successful operation of a heat pipe, which performs passive heat transfer through the natural circulation accompanying the phase change of the fluid. Common indicators for selecting the working fluid include the liquid figure of merit (FOM) and the vapor FOM [24]. The liquid FOM, expressed in Equation (1), is derived based on the pressure balance between the capillary force and the liquid pressure drop in the wick. It provides a quantification of the capillary operating limitations of the heat pipe. Conversely, the vapor FOM, expressed in Equation (2), represents a quantification of the sonic and viscous limits related to the startup of a heat pipe. In certain operating conditions, the successful operation of the heat pipe depends on the vapor's ability to flow from the evaporator to the condenser. Generally, the vapor FOM must reach 1 to initiate the development of continuum flow in the heat pipe [25].

$$M_L = \frac{h_{fg}\rho_l\sigma}{\mu}(\mathrm{W/m^2}), \tag{1}$$

$$M_v = P_v\rho_v(\mathrm{kg/s^2m^4}). \tag{2}$$

Figure 6 illustrates the FOM for both the liquid and vapor phases of several working fluids, including sodium and potassium, which are commonly used in liquid metal heat pipes for microreactors [26]. The primary heat transfer heat pipes generally rely on potassium or sodium to achieve high maximum heat transfer capacities. However, they require high operating temperatures for startup due to their low vapor pressure. For example, a sodium heat pipe generally requires a transition temperature of about 750 K to generate sufficient vapor for effective heat transfer. The primary objective of the design proposed in this paper is to rapidly remove decay heat during accidents, resulting in a more uniform temperature distribution within the monolithic core. Therefore, selecting a working fluid that can work quickly and efficiently to transfer heat from the microreactor core is essential to prevent rapid temperature rise in the core. Therefore, cesium was selected as the working fluid for hybrid heat pipes because of its ability to operate quickly, although it has a lower maximum heat transfer limit compared to sodium and potassium.

Some experiments with cesium heat pipes have been performed at intermediate temperatures. Kemme [27] compared the sonic limitations of liquid metal heat pipes using sodium, potassium, and cesium as working fluids. Their results showed that sonic limitations are mainly influenced by operating temperature and working fluid type. This is because these two factors are closely related to the vapor pressure, which in turn has an effect on the isothermal temperature. Among them, cesium heat pipes were found to operate effectively at lower temperatures, around 350°C. Sodium heat pipes, on the other hand, required temperatures above 500°C to operate. Chen et al. [28] conducted experiments on cesium heat pipes under natural convection cooling conditions. They demonstrated that the theoretical formula for the transition temperature, which predicts sufficient vapor formation for heat transfer inside the heat pipe, corresponded well with experimental results. These results indicated that the transition temperature of cesium heat pipe

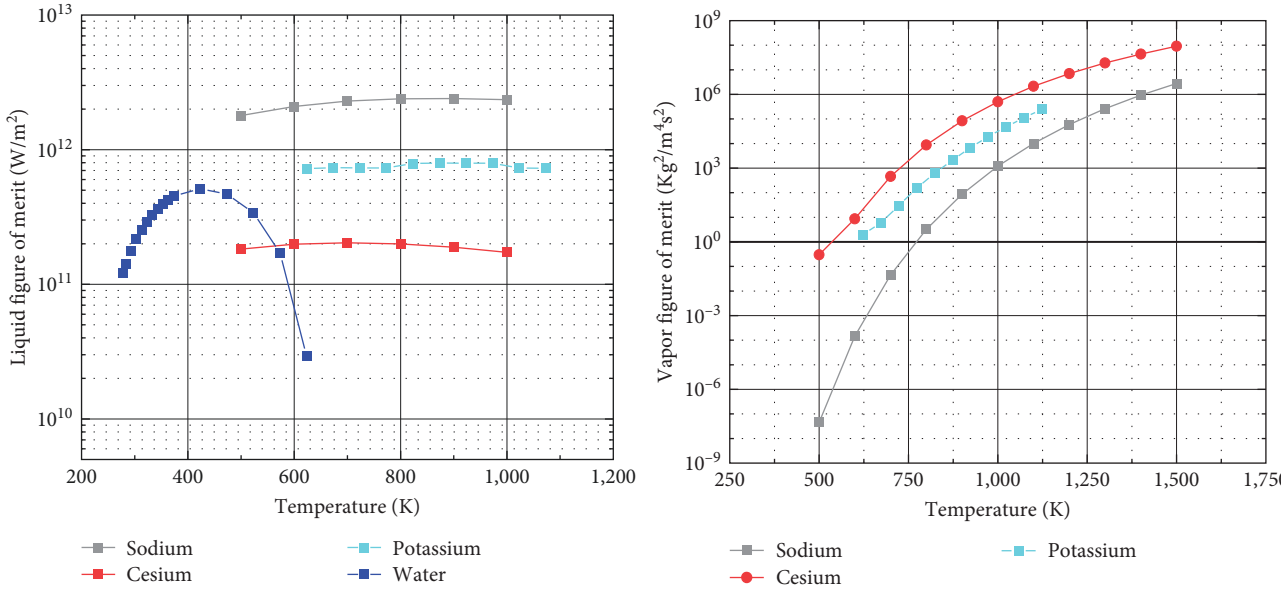


Figure 6: Liquid and vapor figure of merit (FOM) of water and several liquid metals [26].

Table 2: Detailed information of hybrid heat pipe shutdown rod for experiments.

| Index | Parameter | Unit | Value |
|---|---|---|---|
| Envelop | Outer/inner pipe length | mm | 560/300 |
| | Outer/inner pipe diameter | mm | 25.04/15.875 |
| Envelop wick | Outer/inner pipe wall thickness | mm | 1.24/0.89 |
| | Material | — | ASTM 316L |
| | Type | — | Screen (#120) |
| Wick | Porosity | — | 0.634 |
| | Wick thickness | mm | 0.53 |
| Working fluid | Material | — | 99.95% pure cesium |
| Working fluid | Filling amount | G | 50 |
| | Filling ratio | % | 118% |

was ~220°C, while sodium and potassium heat pipes typically operate above 400°C. Therefore, choosing cesium as the working fluid for a hybrid heat pipe is expected to enable rapid heat removal from the monolithic core.

## 3. Set Up for Analysis of Hybrid Heat Pipe Shutdown Rod

*3.1. Manufacturing the Hybrid Heat Pipe Shutdown Rod.* To evaluate the designed passive safety system, scaled-down hybrid heat pipe shutdown bars were fabricated and filled with working fluid. Table 2 summarizes information on the fabricated heat pipes, including the length and dimensions of the outer and inner pipes, which were $L = 560$ mm, $D_o = 25.4$ mm, and $D_i = 15.875$ mm, respectively. The inner tube contained $B_4C$ pellets, which were spring-loaded and sealed, while the outer tube contained a screen wick consisting of six layers of 120 mesh. The inner and outer tubes were joined by welding at the end cap on one side. A filler tube was installed on the other side. The X-ray image of the hybrid heat pipe is shown in Figure 7. In the evaporator section, the neutron absorber was held by a spring, and it was obvious that there was a flow path change area.

*3.2. Experimental Setup.* The thermal performance test of the hybrid cesium heat pipe is shown in Figure 8(a). The evaporator conditions were established using the RF (radio-frequency) induction heating method. This method can provide a range of boundary conditions, including rapid heat transfer changes and high heat flux for conducting operational limit tests. Ambient air was selected as the heat sink for the heat pipe for the investigation of its thermal performance under possible microreactor application conditions. To measure the wall temperature of the heat pipe, a total of five K-type thermocouples and three IR pyrometers were installed along the heat pipe with appropriate spacing, as shown in Figure 8(b). Starting from the beginning of the condenser section, the thermocouples were placed at 50 mm intervals along the side of the heat pipe. To avoid measurement errors caused by the indirect effect of RF heating, IR pyrometers were used to measure the

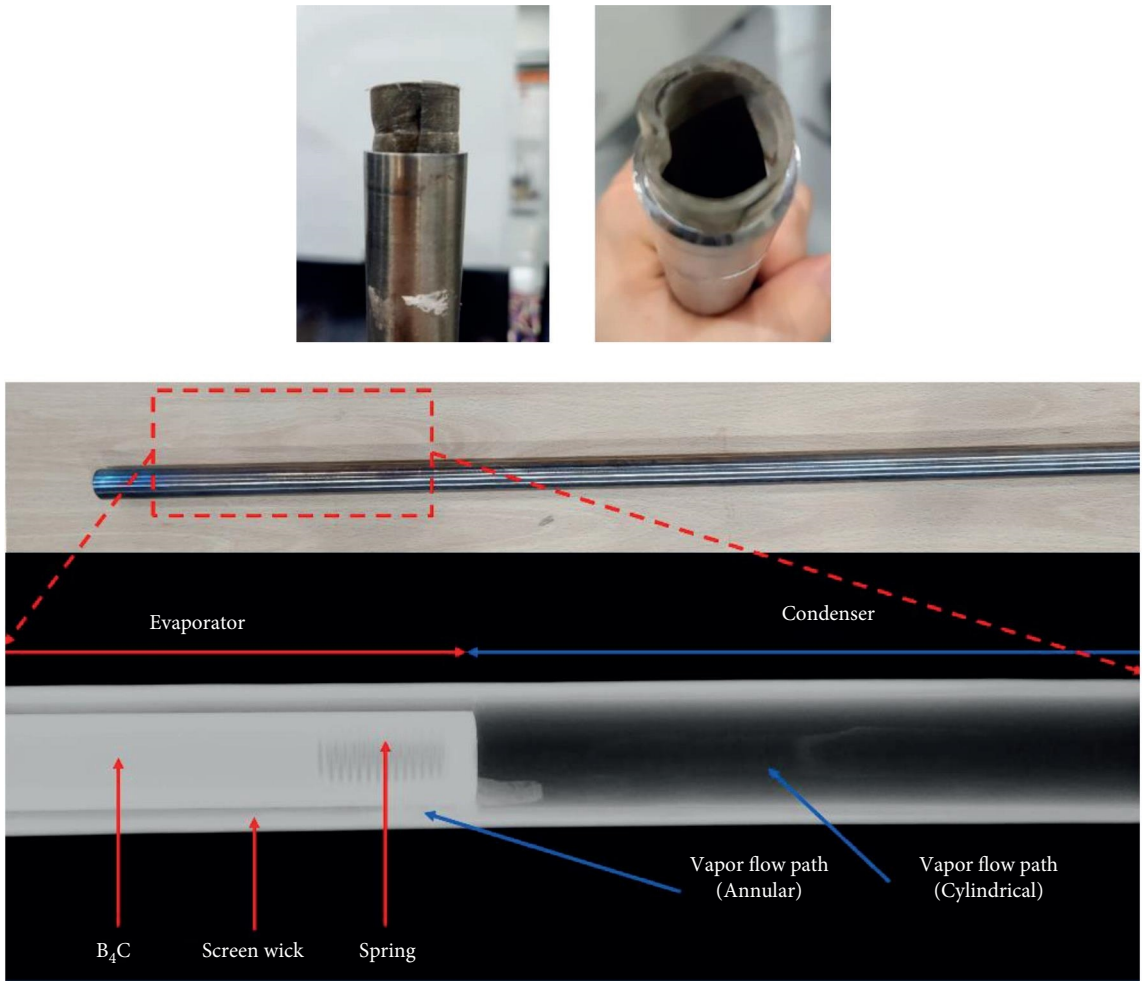


FIGURE 7: X-ray image of hybrid heat pipe at evaporator region.

temperature at three specific points: 50, 150, and 250 mm along the evaporator of the heat pipe. A data acquisition system (Agilent, 34980A) was used to collect all data at 1-s intervals.

To evaluate the heat transfer performance of a hybrid heat pipe, it is important to consider both convective and radiative heat transfer in the total heat transfer rate. The net heat transfer rate can be determined by the sum of the net convection energy rate and the net radiation energy rate, as described in Equations (3), (4), (5), and (6). The Churchill and Chu correlation [29] was used to calculate the heat transfer coefficient. The emissivity of the heat pipe wall was determined by calibrating temperature data obtained from thermocouples and IR thermometers. In the heat balance calculations, an emissivity value is in the range of 0.78–0.81 with a 1.12% uncertainty.

$$\dot{q}_{\text{conv}} = \sum_{i=1}^{n} \pi D_o (x_{i+1} - x_i) h_c (T_i - T_\infty), \tag{3}$$

$$h = \frac{k}{D}\left\{0.60 + \frac{0.387 Ra_D{}^{1/6}}{\left[1 + (0.559/\text{Pr})^{9/16}\right]^{8/27}}\right\}^2, \tag{4}$$

$$\dot{q}_{\text{rad}} = \sum_{i=1}^{n} \sigma \varepsilon \pi D_o (x_{i+1} - x_i)(T_i{}^2 + T_\infty{}^2)(T_i + T_\infty). \tag{5}$$

Table 3 summarizes the test matrix for the hybrid heat pipe feasibility study. The primary objective of this study is to explore the feasibility of the hybrid heat pipe concept, with particular emphasis on its unique geometry that results in changes in the vapor flow area from the evaporator to the condenser. Unlike conventional heat pipes that maintain a constant flow area, the hybrid heat pipe exhibits significant differences between the evaporator and condenser sections. This difference underscores the need to understand the effect of these changes on the isothermal performance of the pipe. Previous studies incorporating structural elements into the evaporator of a heat pipe have emphasized the importance of the flow area characteristics. An experimental study by Kim and Bang [30] introduced a partially concentric annular heat pipe design that includes $B_4C$ as a neutron absorber in the evaporator. This unique geometry was found to significantly change the void ratio between the annular and cylindrical

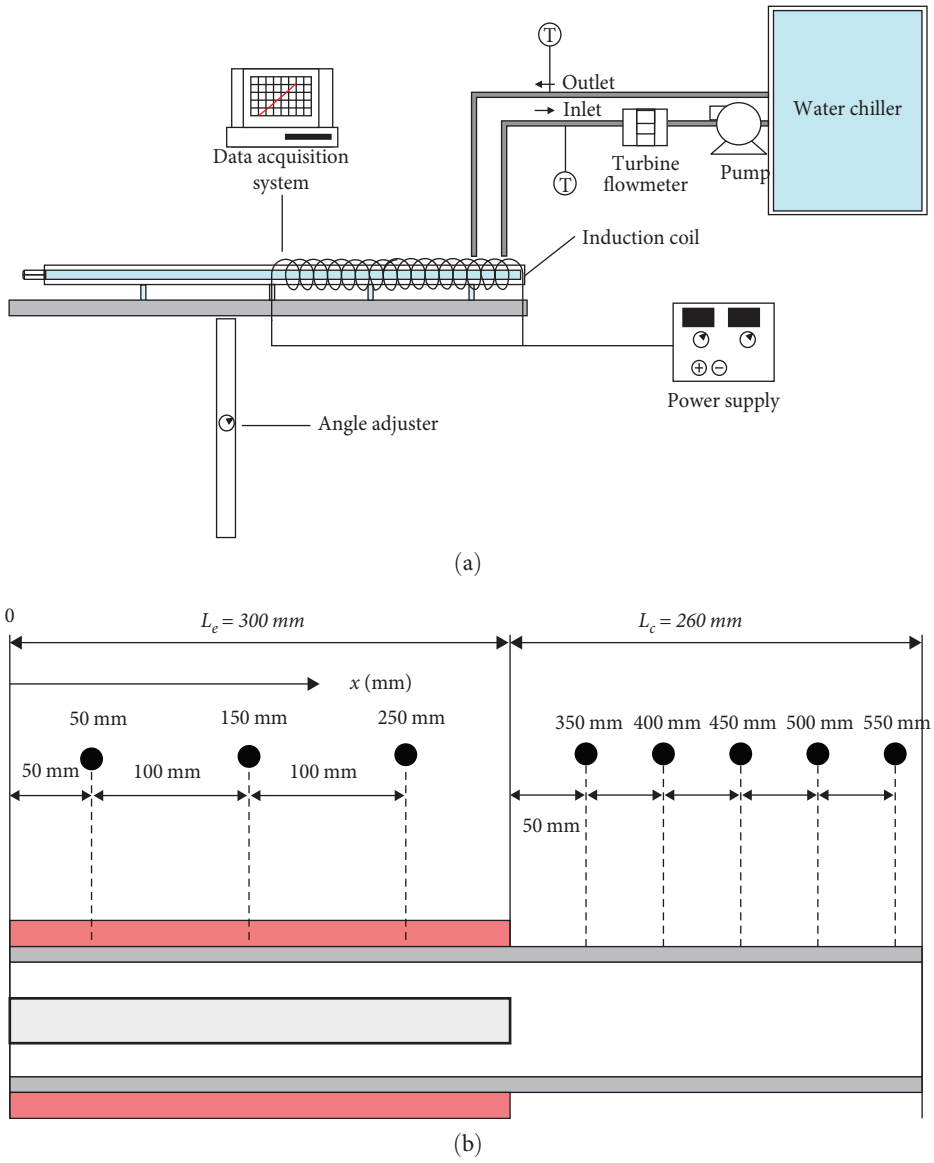


Figure 8: Experimental setup for thermal evaluation of hybrid heat pipe: (a) configuration of heat pipe test facility and (b) temperature measurement points.

Table 3: Test matrix for evaluation of feasibility of hybrid heat pipe shutdown rod.

| Test | Purpose | Test conditions | |
|---|---|---|---|
| Startup | At each heat input, evaluate whether the heat pipe is operating properly without startup problems | $q_{1s}$ | $120.8 \pm 5.3$ W |
| | | $q_{2s}$ | $228.1 \pm 9.9$ W |
| | | $q_{3s}$ | $254.4 \pm 11.1$ W |
| Operating limit | Investigate maximum heat transfer capacity that the cesium heat pipe could remove by gradually increasing heat input until the operating limit was reached | $q_{1o}$ | $69.3 \pm 2.7$ W |
| | | $q_{2o}$ | $161.6 \pm 7.0$ W |
| | | $q_{3o}$ | $205.5 \pm 8.9$ W |
| | | $q_{4o}$ | $269.4 \pm 12.7$ W |
| | | $q_{5o}$ | $308.8 \pm 14.5$ W |

flow regions, which affects the surface velocity of the liquid film and vapor. Therefore, it is necessary to redefine the surface velocity to accurately model the immersion limit based on the maximum relative velocity between the vapor and liquid. Furthermore, Mueller and Tsvetkov [31] proposed the concept of placing the fuel in the center of the evaporator of a partially concentric annular heat pipe. The study highlighted the complexities associated with changes

in the vapor flow region on the sonic speed limit, noting that both area and mass additions can independently contribute to flow choking. Therefore, unique designs require a comprehensive analysis of the heat transfer characteristics.

The purpose of this study is to investigate the thermal characteristics and rapid operability of a hybrid cesium heat pipe. Although there have been experimental studies on cesium heat pipes, the unique geometry of our proposed design, with a change in the vapor flow area between the evaporator and the condenser, requires an investigation of its heat transfer characteristics. To accomplish these goals, we chose to conduct a startup test and an operating limit test. The startup test examines the feasibility of the hybrid heat pipe to ensure that it operates successfully at each heat input level without startup problems. To determine the maximum heat transfer capacity of the cesium heat pipe, the operating limit tests were performed by gradually increasing the heat input until dry-out occurred. To evaluate whether the operating limits of hybrid heat pipes with unusual geometries can be predicted by existing models, these results were used to compare with operating limit models. We controlled the power with current levels that started at 10 A and increased by 3 A at each step from the frozen start to the operating limit. The experiment was considered a steady state when the temperature remained within 5°C for 10 min. The experiment was terminated when the operating limit was reached, indicated by a large temperature difference between the evaporator and condenser, a phenomenon known as partial dry-out. By integrating the uncertainty in the surface temperature using Equations (6), (7), and (8), the maximum uncertainty in the heat transfer rate was determined. Table 3 evaluates the uncertainties for all experimental cases.

$$\partial \dot{q}_{\mathrm{rad}} = \sqrt{\left(\frac{\partial \dot{q}_{\mathrm{rad}}}{\partial D}\right)^2 \partial D^2 + \left(\frac{\partial \dot{q}_{\mathrm{rad}}}{\partial x}\right)^2 \partial x^2 + \left(\frac{\partial \dot{q}_{\mathrm{rad}}}{\partial \xi}\right)^2 \partial \xi^2 + \left(\frac{\partial \dot{q}_{\mathrm{rad}}}{\partial T_i}\right)^2 \partial {T_i}^2 + \left(\frac{\partial \dot{q}_{\mathrm{rad}}}{\partial T_\infty}\right)^2 \partial {T_\infty}^2}, \tag{6}$$

$$\partial \dot{q}_{\mathrm{conv}} = \sqrt{\left(\frac{\partial \dot{q}_{\mathrm{conv}}}{\partial D}\right)^2 \partial D^2 + \left(\frac{\partial \dot{q}_{\mathrm{conv}}}{\partial x}\right)^2 \partial x^2 + \left(\frac{\partial \dot{q}_{\mathrm{conv}}}{\partial h_c}\right)^2 \partial {h_c}^2 + \left(\frac{\partial \dot{q}_{\mathrm{conv}}}{\partial T_i}\right)^2 \partial {T_i}^2 + \left(\frac{\partial \dot{q}_{\mathrm{conv}}}{\partial T_\infty}\right)^2 \partial {T_\infty}^2}, \tag{7}$$

$$\partial \dot{q}_{\mathrm{HP,Cooling}} = \sqrt{\left(\frac{\partial \dot{q}_{\mathrm{HP,Cooling}}}{\partial \dot{q}_{\mathrm{rad},a}}\right)^2 \partial \dot{q}^2{}_{\mathrm{rad},a} + \left(\frac{\partial \dot{q}_{\mathrm{HP,Cooling}}}{\partial \dot{q}_{\mathrm{conv},c}}\right)^2 \partial \dot{q}^2{}_{\mathrm{conv},c} + \left(\frac{\partial \dot{q}_{\mathrm{HP,Cooling}}}{\partial \dot{q}_{\mathrm{rad},c}}\right)^2 \partial \dot{q}^2{}_{\mathrm{rad},c}}. \tag{8}$$

## 4. Results and Discussions

*4.1. Startup Test of Hybrid Cesium Heat Pipe.* The hybrid heat pipe, designed as a passive safety system for microreactors, is intended to operate effectively at low temperatures. For this reason, cesium is used as the working fluid to facilitate rapid operation at low temperatures. However, the unique geometry of the hybrid heat pipe, characterized by a variable vapor diameter due to the presence of a neutron absorber in the evaporator, requires extensive feasibility testing. To assess this feasibility, the startup temperature performance was investigated. These tests focused on the temperature behavior from a frozen start, a critical aspect for liquid metal heat pipes. Due to their low vapor pressures compared to water, liquid metals such as sodium and potassium often face startup problems. For the successful operation of the hybrid heat pipe, establishing a continuous vapor flow is essential. This is necessary to achieve an isothermal axial temperature distribution. Vapor flow patterns in liquid metal heat pipes are categorized into three types: rarefied, transition, and continuum flows, determined by the transition temperature ($T_{\mathrm{tr}}$) as outlined in Equation (9) [32]. The Knudsen number ($Kn$), a critical dimensionless parameter, dictates the vapor state within the heat pipe. $Kn$ is defined as the ratio of the mean free path of the vapor molecules ($\lambda$) to a significant physical dimension of the system, typically the diameter of the heat pipe ($D_v$), and is expressed mathematically as Equation (10). When $Kn > 0.1$, the heat pipe is considered to be in a rarefied flow state, where there is insufficient cesium vapor to maintain a uniform temperature distribution. Conversely, when $Kn < 0.01$, the vapor is in a continuous flow state, with enough cesium vapor generated to allow for an isothermal temperature profile. The Clausius–Clapeyron equation, which describes the relationship between the saturation temperature and saturation pressure of a vapor, plays a significant role in evaluating the transition temperature, as expressed in Equation (12). Based on the diameter of the condenser region, the transition temperature necessary for establishing continuous vapor flow in the hybrid heat pipe design was determined to be 205.1°C. This temperature is ~270°C lower than that expected when sodium is used as the working fluid, highlighting the efficiency of the hybrid design at lower operating temperatures.

$$T_{\mathrm{tr}} = \frac{\sqrt{2}\pi {\sigma_v}^2 P_{\mathrm{sat}}(T_{\mathrm{tr}}) Kn(0.01)}{1.051 k_B} D_v, \tag{9}$$

where $k_B$ is a Boltzmann constant, $\sigma_v$ is a collision diameter of cesium atom.

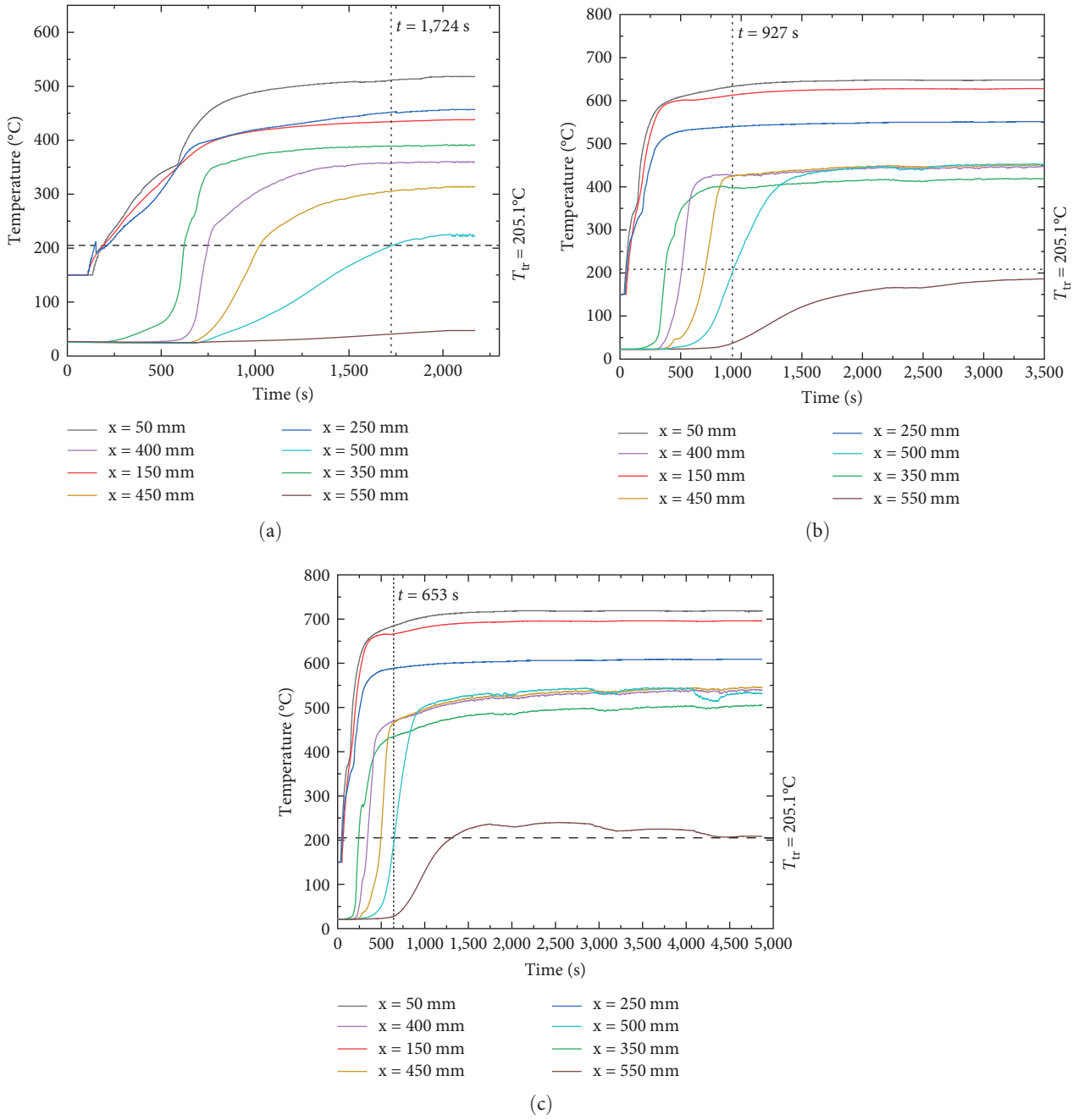


FIGURE 9: Startup temperature behavior of hybrid heat pipe according to the heat transfer rates: (a) $q_{1s} = 120.8\ W$; (b) $q_{2s} = 228.1\ W$; and (c) $q_{3s} = 254.4\ W$.

$$Kn = \frac{\lambda}{D_v}, \tag{10}$$

$$\lambda = \frac{1.051 k_B T}{\sqrt{2}\pi {\sigma_v}^2 P}, \tag{11}$$

$$P_{sat}(T_{tr}) = \log(9.04269 - 3784.02/T_{tr}). \tag{12}$$

Figure 9 illustrates the startup temperature distribution according to the heat transfer rate of the hybrid heat pipe. The experimental results show that the heat pipe quickly exceeded the predicted transition temperature during startup. When the heat transfer rate reached 120.8 W, the hybrid heat pipe began to operate, causing the temperature to rise in the axial direction. At $x = 500$ mm in $q_{1s}$, the temperature rose to about 221°C, which is close to the transition temperature, indicating that the continuum flow developed around the 500 mm region. When the heat input increased to $q_{2s}$, the temperature at this point rose to ~431.2°C, and in $q_{3s}$ to ~532.4°C. The results demonstrate that the hybrid cesium heat pipe can quickly form a continuous flow at low temperatures and effectively transfer phase change heat in the axial direction once sufficient vapor flow is established. It was also observed that

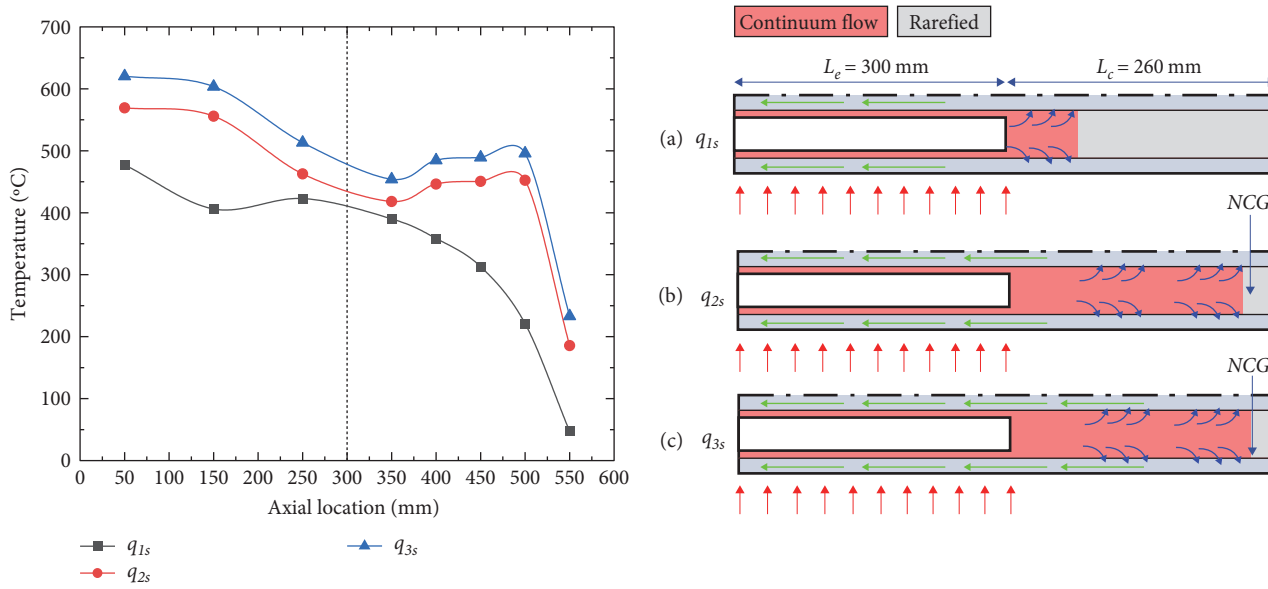


FIGURE 10: Steady state temperature distribution and schematic of continuum flow development of hybrid heat pipe.

TABLE 4: Temperature changes in the evaporator and the condenser due to the converging–diverging effect.

| | Temperature drop (K) ($T_{150}$–$T_{250\ mm}$) | Temperature recovery (K) ($T_{450}$–$T_{350\ mm}$) | Continuum flow developed length ($T_x > 205.1$°C) |
|---|---|---|---|
| $q_1$ | 71.2 | 16.8 | $x = 450$ mm |
| $q_2$ | 151.14 | 34.4 | $x = 500$ mm |
| $q_3$ | 166.45 | 41.8 | $x = 500$ mm |

the startup time required to achieve continuous flow to the condenser section decreased significantly as the heat input increased. For example, in $q_{1s}$, it took 1,724 s to reach the transition temperature at 500 mm to achieve continuum flow. This decreased to 927 s in $q_{2s}$ and further decreased to 653 s in $q_{3s}$, indicating that as the heat input increased, the heat pipe activated the condenser section more rapidly.

Figure 10 shows the steady-state temperature distribution in the hybrid heat pipe. The graph indicates that as the hybrid heat pipe operates, there is a significant increase in temperature at the condenser. Except for the point at $x = 550$ mm, there is an extension of an isothermal temperature distribution from 350 to 500 mm. This extension becomes more pronounced as the heat input increases. This observation confirms that the hybrid heat pipe can operate at low heat input to transfer latent heat to the condenser. Figure 10 illustrates the onset of operation of the hybrid heat pipe, demonstrating how the vapor flow, which carries latent heat, moves into the condenser region as the heat input increases. As the heat transfer rate increases from $q_{1s}$ to $q_{3s}$, the continuum flow expands further into the condenser, leading to a more uniform temperature distribution. However, a significant increase in the heat transfer rate does not result in a notable temperature change at $x = 550$ mm due to the presence of noncondensable gases at the end of the condenser, preventing the cesium vapor from fully reaching this area, despite some degree of compression as the heat input increases.

*4.2. Geometry Effect of Hybrid Heat Pipe.* The unique geometry of the proposed hybrid heat pipe design, which incorporates changes in the vapor flow area between the evaporator and condenser, plays an important role in the thermal performance of the heat pipe. Generally, the isothermal temperature of a heat pipe is influenced by sufficient vapor flow to transfer latent heat. Thus, the variation of flow area in the hybrid heat pipe design significantly affects the vapor flow dynamics, resulting in unique thermal behavior. An important finding from the experimental results is that there are two distinct temperature gradients within the hybrid heat pipe. First, unlike typical liquid metal heat pipes that remain at an isothermal temperature until dry-out, the hybrid heat pipes exhibit a significant temperature gradient along the axial direction within the evaporator even without reaching dry-out. Once the hybrid heat pipe begins to activate up to the condenser, a significant axial temperature decrease is observed inside the evaporator, especially at the evaporator outlet. Second, an increase in temperature is observed as the cesium vapor travels to the condenser, contrasting with the axial temperature decrease in the evaporator. The temperature at the 350 mm point remains consistently lower than the temperature observed above 400 mm. These significant temperature changes in opposite directions at the evaporator and condenser highlight the unique characteristics of the hybrid heat pipe design. Table 4 summarizes the evaporator temperature drop and condenser temperature recovery in a hybrid heat pipe. After a developed continuum flow is

formed, a large temperature gradient appears, and both the temperature drop in the evaporator and the temperature recovery in the condenser increase as the heat transfer rate increases.

This phenomenon is explained by the converging–diverging nozzle effect, often observed in liquid metal heat pipes where the boundary conditions consist of an evaporator and condenser section [33, 34, 35, 36, 37]. In a heat pipe, despite a constant cross-sectional area, mass is added at the evaporator and removed at the condenser. This results in a variable mass flow that causes velocity changes, similar to the flow dynamics observed in converging–diverging nozzles where the velocity changes due to variations in cross-sectional area. This behavior is particularly prevalent in heat pipes using low vapor pressure working fluids such as sodium and lithium. At startup, the low vapor density causes the vapor to reach velocities near the sonic limit, significantly affecting the temperature gradient due to the converging–diverging effect. However, liquid cesium, with its relatively high vapor pressure, mitigates the effect of mass flow rate variations on vapor velocity, thereby reducing the significance of the converging–diverging effect in heat pipes. For example, a sodium heat pipe consisting only of an evaporator and condenser section exhibited a distinct converging–diverging effect in temperature distribution [27]. This was characterized by a temperature drop of about 100 K at the evaporator and temperature recovery after the condenser inlet. In contrast, a cesium heat pipe exhibits good isothermal performance with no significant temperature gradient prior to dry-out, representing a temperature change of about 20 K across the effective length of the heat pipe [28].

However, both the phase change and the change in flow area can affect the vapor velocity in a hybrid heat pipe. This means that the hybrid heat pipe must consider not only the phase change but also the flow area variation, resulting in a distinct converging–diverging effect not observed in conventional designs when cesium is used as the working fluid. The two distinct temperature gradients within the temperature distribution of a hybrid heat pipe are caused by these effects. The converging effect starts in the evaporator section, and the mass flow rate increases and the maximum flow rate occurs at the evaporator outlet. This is accompanied by a significant increase in vapor velocity, which peaks at the evaporator outlet. An important aspect of this region is that the vapor pressure decreases to balance the force–momentum. As the vapor velocity increases rapidly from the evaporator inlet to the outlet, the pressure decreases. Because hybrid heat pipes have a small vapor diameter in the evaporator due to the neutron absorber, the vapor flow can be easily accelerated from the inlet to the outlet. As the vapor pressure decreases, the wall temperature distribution forms a gradient, and this effect becomes more pronounced as the heat input increases. When the vapor enters the condenser section, it transitions to the diverging phase. The vapor begins to condense, resulting in a decrease in mass flow. This results in a decrease in velocity, and the pressure begins to recover. Since the velocity reduction can be affected by both the expansion of the flow area and condensation, it is important to consider the condensation effect alongside the changes in the flow area within the hybrid heat pipe. This

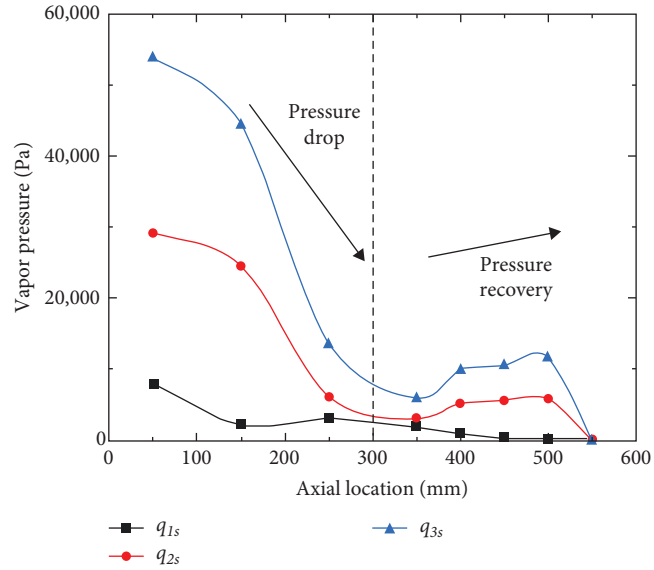


FIGURE 11: Evaluated vapor pressure distribution in hybrid heat pipe according to heat transfer rate.

aspect is especially important when comparing the magnitude of the pressure drop in the evaporator with the pressure recovery, in the condenser section. In the evaporator, the flow area does not change, and only the converging effect of adding mass flow is observed, whereas, in the condenser section, the flow is affected by changes in the flow area and condensation. Therefore, understanding the effect of the hybrid heat pipe geometry on pressure drop and recovery is essential. Although it is difficult to directly measure the pressure distribution in a liquid metal heat pipe, this study utilized wall temperature data and a thermal resistance model to indirectly estimate the vapor pressure distribution in a hybrid heat pipe. By using the relationship between saturation temperature and saturation pressure as described by the Clausius-Clapeyron equation, the vapor pressure distribution can be approximated from steady-state temperature data using Equations (13), (14), (15), and (16) and can provide insights into how the pressure changes with varying heat input.

$$T_{v,\mathrm{eva},i} = T_{\mathrm{wall},i} - Q\left(R_{\mathrm{wall},i} + R_{\mathrm{wick},i}\right), \tag{13}$$

$$T_{v,\mathrm{con},i} = T_{\mathrm{wall},i} + Q\left(R_{\mathrm{wall},i} + R_{\mathrm{wick},i}\right), \tag{14}$$

$$R_{\mathrm{wall},i} = \frac{\ln(D_o/D_i)}{2\pi k_w L_i}, \tag{15}$$

$$R_{\mathrm{wick},i} = \frac{\ln(D_i/D_v)}{2\pi k_{\mathrm{eff}} L_i}. \tag{16}$$

Figure 11 shows the evaluated static pressure distribution of the hybrid heat pipe based on the wall temperature. In the evaporator, a significant pressure drop is observed from the inlet to the outlet. In contrast, the condenser section shows only a slight pressure recovery immediately after the evaporator

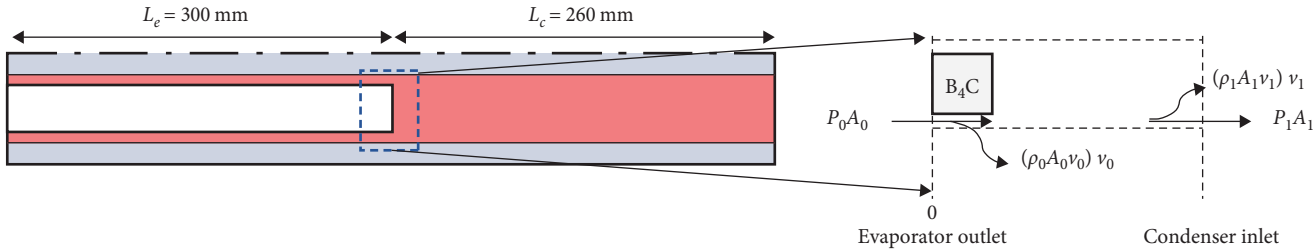


FIGURE 12: Control volume for analyzing momentum balance during flow area variation.

outlet, which is much less than the drop observed in the evaporator, and this trend becomes more pronounced as the heat transfer increases. This implies that increased vapor generation in the evaporator results in a more marked converging–diverging effect in the hybrid heat pipe. The behavior of pressure drops is similar to the converging effect in a sodium heat pipe; however, the pressure recovery in the condenser part is significantly different in a hybrid heat pipe. The presence of a neutron absorber, which reduces the flow area and consequently increases the vapor velocity for the same mass flow rate, is responsible for the significant pressure drop observed in the hybrid heat pipe evaporator. However, as the vapor enters the condenser, the vapor velocity changes due to the combined effect of condensation and expansion of the flow area. As a result, pressure recovery is less pronounced than in the evaporator.

To evaluate the effect of flow area changes on pressure recovery, a theoretical analysis was performed focusing on the pressure ratio between two locations, represented as $P_0/P_1$. Since the wall temperature is determined by the static vapor pressure, the method of using the static pressure ratio evaluation of the temperature drop along the evaporator is commonly used in heat pipe analysis. This involved performing a steady-state force–momentum balance within a specified control volume, as shown in Figure 12. This analysis included several assumptions, primarily emphasizing the effect of inertia and considering the effect of friction to be negligible because when the heat pipe has developed a continuous flow that is sufficiently capable of transferring the phase change in the axial direction, the inertial effect will dominate over the fractional effect due to the high evaporation rate of the heat pipe [33, 38]. The force–momentum balance between the two locations in the control volume was then characterized using Equations (17) and (18).

$$P_0A_0 + (\rho_0A_0v_0)v_0 = P_1A_1 + (\rho_1A_1v_1)v_1, \tag{17}$$

$$\frac{P_0A_0}{P_1A_1} + \left(\frac{A_0}{A_1}\right)\left(\frac{P_0}{P_1}\right)\frac{(\rho_0v_0)v_0}{P_0} = 1 + \frac{(\rho_1v_1)v_1}{P_1}. \tag{18}$$

In these equations, the vapor is assumed to behave as an ideal gas, where $R$ is the gas constant. The Mach number is replaced with velocity in the calculations.

$$P = \rho RT, \tag{19}$$

$$v^* = \sqrt{\gamma RT}, \tag{20}$$

$$M = v/v^*. \tag{21}$$

Consequently, the pressure ratio between two locations can be evaluated using Equation (22).

$$\frac{P_0}{P_1} = \left(\frac{A_1}{A_0}\right)\left(\frac{1+\gamma M_1{}^2}{1+\gamma M_0{}^2}\right). \tag{22}$$

In the flow area variation region, as shown in the control volume in Figure 12, the analysis assumes that the highest cesium velocity occurs at the evaporator outlet, where $M_0$ is approximately equal to 1. This assumption allows the relationship between the flow area variation and the pressure ratio of the evaporator outlet and condenser inlet to be evaluated, as described by Equation (23).

$$\frac{P_0}{P_1} = \left(\frac{A_1}{A_0}\right)\left(\frac{1+\gamma M_1{}^2}{1+\gamma}\right). \tag{23}$$

Figure 13 illustrates the effect of changes in flow area and Mach number at the condenser inlet on the pressure recovery ratio. The analysis shows that the difference in vapor velocity between the evaporator and condenser increases the pressure recovery, meaning that an increase in pressure is induced to compensate for the force–momentum generated by the decrease in vapor velocity leaving the evaporator. As the velocity drop is minimized, the pressure ratio tends to remain close to 1, indicating that no significant pressure drop occurs. As a result, the converging–diverging effect is most pronounced in heat pipes where the boundary conditions consist of the evaporator and condenser rather than the adiabatic section. The analysis also reveals that the pressure recovery decreases due to the expansion of the flow area. Specifically, the flow change ratio ($A_1/A_0$) for the hybrid heat pipe is found to be 2.4, indicating less pressure recovery for force–momentum balance as velocity decreases compared to a heat pipe with a uniform flow area. Consequently, the analysis indicates that the lower pressure recovery observed in the condenser, compared to the pressure drop in the evaporator, is due to the effect of flow change. Therefore, as seen in the results in Figure 13, the significant pressure drop in the evaporator and the lower pressure recovery in the condenser of the hybrid heat pipe are due to its unique geometry. The significant pressure drop results from the

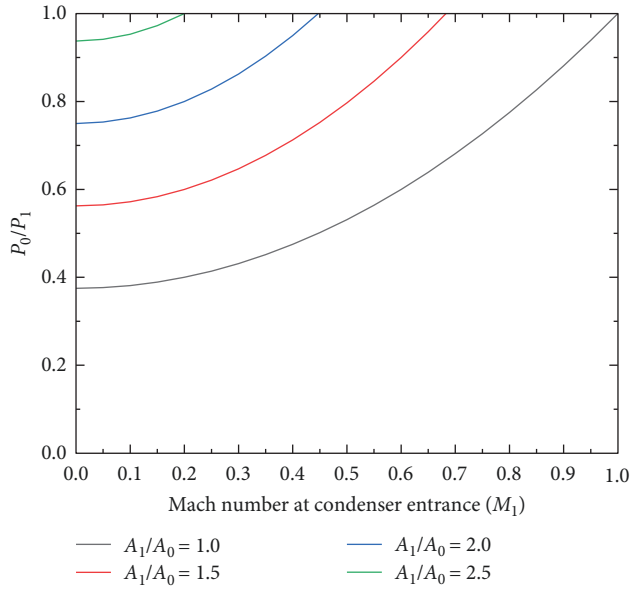


FIGURE 13: Pressure ratio between evaporator outlet and condenser inlet according to flow area variation and velocity.

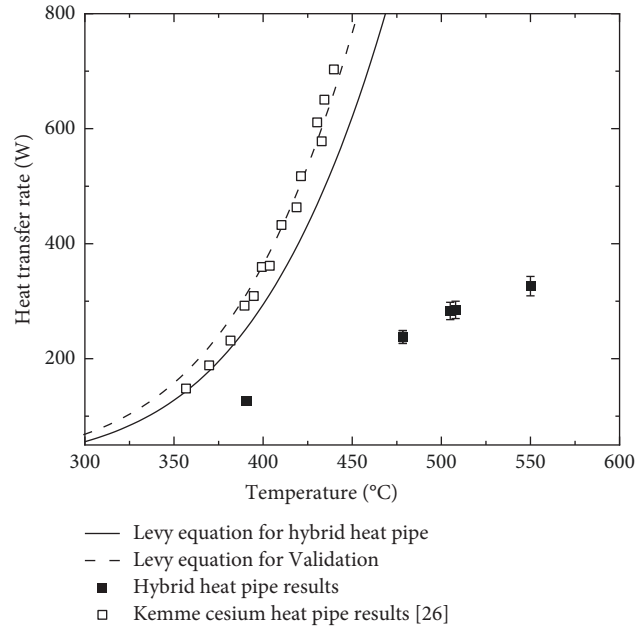


FIGURE 14: Comparison of sonic limit and heat transfer rate of hybrid heat pipe.

formation of high velocities in a narrow flow region, creating a noticeable converging effect. Conversely, the relatively small pressure recovery in the condenser is due to the change in flow area, which reduces the effectiveness of pressure recovery. As a result, the pressure distribution characteristics of the hybrid heat pipe are attributed to the enhancement of the converging–diverging nozzle effect due to its structural features, manifested as a sharp pressure drop at the evaporator and a small pressure recovery at the condenser. This is reflected in the wall temperature distribution, where a significant temperature decrease is observed in the evaporator in the range $x = 150$ mm to $x = 250$ mm. The temperature increase in the condenser region is relatively small, especially between $x = 350$ mm and $x = 400$ mm, where the vapor velocity changes due to flow expansion and condensation.

*4.3. Sonic Limit Evaluation of Hybrid Heat Pipe.* In typical cylindrical cesium heat pipes, the converging–diverging effect is minimal, resulting in no significant temperature gradient until dry-out [28, 39]. In contrast, in sodium heat pipes, the converging–diverging phenomenon occurs. However, the hybrid heat pipe exhibits an enhanced converging–diverging effect due to its structural characteristics, leading to a notable temperature gradient even when cesium is used as the working fluid. Based on experimental results and theoretical analysis, it has been established that the thermal behavior of a hybrid heat pipe is characterized by a significant pressure drop in the evaporator, primarily due to the presence of a neutron absorber, and a relatively modest pressure recovery in the condenser, attributable to flow area variations. A major concern during the startup phase of a liquid metal heat pipe is the potential risk of reaching the sonic limit. This phenomenon typically occurs when vapor velocity nears the speed of sound, creating a bottleneck that substantially impedes vapor movement from the evaporator to the condenser. A primary contributing factor is the high-flow velocity at the evaporator exit, which, when coupled with low back pressure in the condenser indicating poor pressure recovery, becomes particularly problematic. This scenario is common in hybrid heat pipes where the narrow flow area of the evaporator causes high velocities, and flow variations make it easy for low-pressure recovery to occur in the condenser region. Given the unique startup characteristics of hybrid heat pipes, investigating the sonic limit, especially for safety systems in microreactors, is essential. Experimentally assessing this limit involves a careful analysis of temperature variations in the evaporator, which may be influenced by changes in the condenser's boundary conditions affecting back pressure. However, in the case of hybrid heat pipes, air natural convection is chosen for cooling to minimize the increase in system size, making controlling the condenser boundary condition challenging. Therefore, the analysis of the sonic limit is conducted by comparing the heat transfer rate with the criteria outlined in the Levy and Chou [40] model as outlined in Equation (24). This approach provides a practical method to evaluate the sonic limit.

$$Q = \frac{\rho_v v_S h_{fg}}{\sqrt{2(\gamma + 1)}} A_v. \tag{24}$$

Figure 14 presents a comparison between experimental heat transfer rates and the sonic limit. To validate the Levy model, these results were compared with data from previous cesium heat pipe experiments [27]. The results indicate that under all experimental conditions, the hybrid heat pipe consistently requires a lower heat transfer rate to reach the sonic limit. This finding suggests that the proposed hybrid heat pipe does not experience any problems during the startup

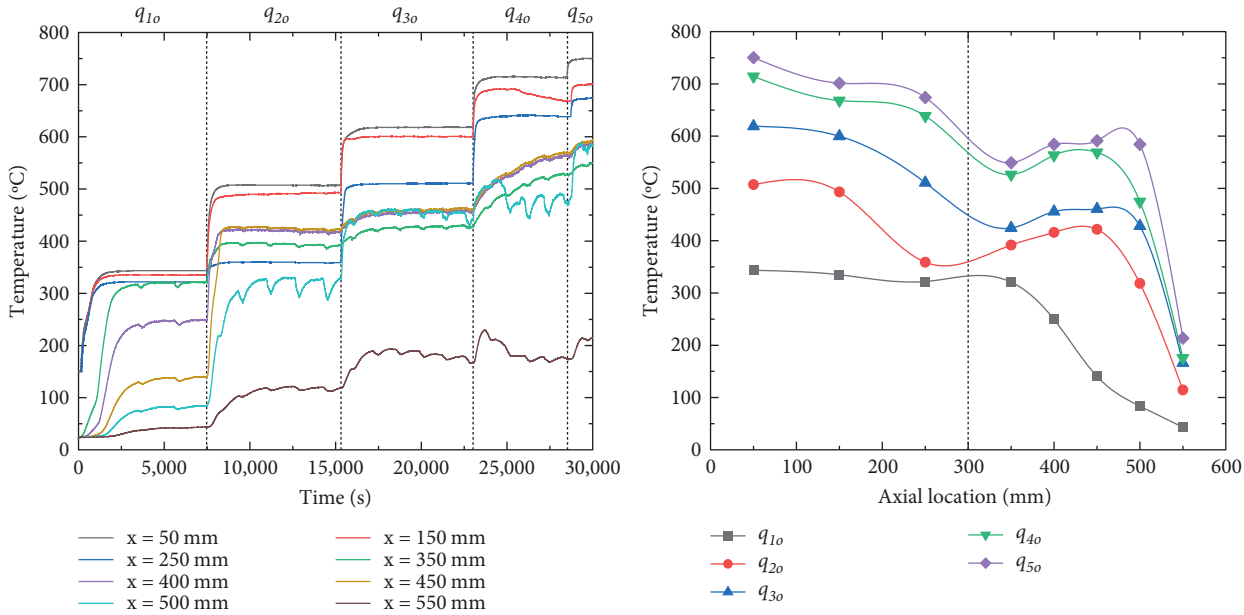


FIGURE 15: Temperature distribution of hybrid heat pipe from startup to partial dry out.

process in conducting heat efficiently in the axial direction. Despite the significant pressure drop in the evaporator and the relatively low back pressure, both consequences of the hybrid heat pipe's unique geometry, this design effectively maintains a high vapor pressure to prevent excessive velocity at the evaporator. Additionally, operating the condenser under natural convection enables the heat transfer rate to self-adjust, thereby preventing choked flow. These two design choices, the selection of the working fluid and the condenser boundary conditions lead to a back pressure that increases with rising power levels, demonstrating the effective use of liquid cesium as the working fluid in this heat pipe configuration, even with its structural constraints.

*4.4. Capillary Limit of Hybrid Heat Pipe.* The hybrid heat pipe discussed in this paper is a scaled-down model designed to investigate its thermal characteristics at the lab scale. For its application in microreactors, an operating limit model is employed for full-scale design. Operating limit models are crucial tools for microreactor design, determining the maximum heat capacity and number of heat pipes that can be effectively managed to achieve the desired capacity. Therefore, evaluating whether the maximum heat transfer rate of the hybrid heat pipe is in good agreement with operating limit models is essential. This evaluation is particularly important due to the unique structural features of the hybrid heat pipe, which distinguish its geometry from conventional heat pipes and result in an enhanced converging–diverging effect. The goal is to compare the maximum heat transfer rate of a hybrid heat pipe operating under horizontal conditions to existing models of operating limitations, particularly focusing on the dry-out limit. The tests were conducted by progressively increasing the RF current input until dry-out or partial dry-out occurred.

As shown in Figure 15, it was observed that the temperature along the axial direction of the hybrid heat pipe increased with the operation, except at the 550 mm point, where the presence of non-condensable gases limited the cesium vapor reach, and the temperature gradient between $x = 150$ mm and $x = 250$ mm in the hybrid heat pipe is influenced by the low back pressure at the condenser, a characteristic feature of this design. On the other hand, the evaporator inlet region between $x = 50$ mm and $x = 150$ mm is less affected by the low back pressure, and the flow area remains constant, similar to a cylindrical heat pipe. This results in a stable flow that prevents the development of a temperature gradient until partial dry-out occurs.

From $q_{1o}$ to $q_{3o}$, the hybrid heat pipe shows a relatively small temperature difference between $x = 50$ mm and $x = 150$ mm, suggesting stable operation. However, as the heat input increases, this temperature difference becomes more pronounced. In particular, the temperature difference rises sharply to 46.2°C in the $q_{4o}$ and intensifies to ~51.4°C in the $q_{5o}$. This significant increase in temperature difference at the evaporator entrance indicates the onset of partial dry out, which is induced by the partial fluid depletion within the heat pipe. Dry-out due to fluid depletion is caused by entrainment limit or capillary limit. Capillary limit occurs when the maximum fluid transport by the wick structure cannot keep up with the evaporation rate. The entrainment limit can also cause the evaporator to dry out if the vapor flow is fast enough to disturb the liquid returning to the evaporator. This appears as temperature fluctuations in the condenser and is generally more common at inclined angles and under intense cooling conditions [34]. In experiment results, it did not represent temperature fluctuations caused by vapor dragging the returning liquid in the temperature distribution, therefore, determined that the cause of the

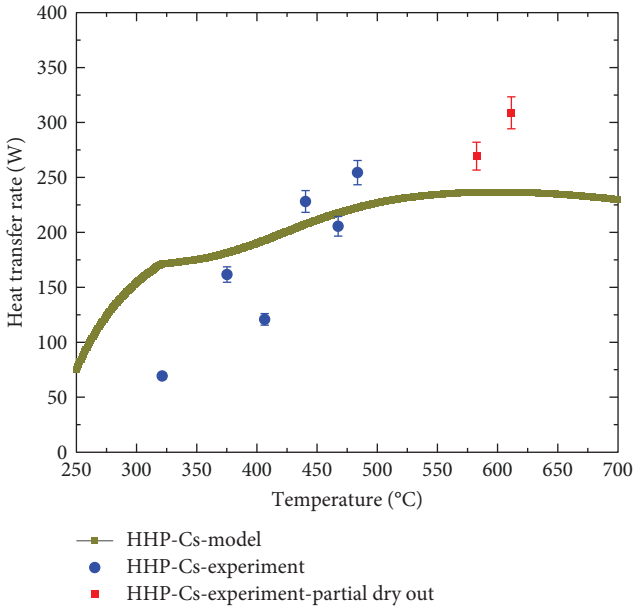


FIGURE 16: Comparison of the heat transfer rate results with operating limit model.

partial dry out was the capillary limit. This means that the capillary forces are not enough to effectively transport the fluid to the inlet of the evaporator. As a result, this leads to a temperature gradient similar to the dry-out phenomenon commonly observed in conventional heat pipes. This tendency continues to intensify as the heat input increases, eventually leading to complete desiccation that cannot provide phase change heat transfer.

The theoretical capillary limit is evaluated using the Chi model, a well-established capillary model [41], as outlined in Equation (25). This expression calculates the heat transfer rate at which the maximum heat transfer rate of liquid transpiration supported by the wick configuration is able to overcome the resistance of the flow. Figure 16 shows a comparison between the experimentally measured heat transfer rate and the predictions of the boundary condition model. This comparison shows that the capillary limit model can effectively distinguish between normal operation and partial dry-out despite the unique internal structure of the hybrid heat pipe. In particular, the maximum difference at the point where partial dry-out occurs is about 28.3% compared to the model prediction. It means that despite the variation of the flow area, the operating limit model can be effectively applied to the design of the hybrid heat pipe. The reason is that the geometry of the hybrid heat pipe mainly affects the vapor flow, while it has a small effect on the liquid flow area. In general, the resistance to liquid flow is much greater than the resistance to vapor flow. Therefore, even though the vapor flow path of a hybrid heat pipe is different from that of a conventional heat pipe, the capillary model is still an effective tool for predicting the heat transfer rate of a hybrid heat pipe. This effect is mainly due to the similarity in wick flow area and fluid flow resistance between hybrid heat pipes and cylindrical heat pipes.

$$Q_{\text{capillary}} = \frac{2\sigma\left(\frac{1}{r_{\text{eff}}}\right)}{L_{\text{eff}}\left(F_{v,\text{av}} + F_{l,\text{av}}\right)} \approx \frac{2\sigma\left(\frac{1}{r_{\text{eff}}}\right)}{L_{\text{eff}}F_{l,\text{av}}}. \tag{25}$$

## 5. Conclusions and Future Work

To reduce the thermal gradient on the monolith core of a microreactor, a new safety system concept has been proposed that replaces the conventional shutdown rod with a hybrid shutdown rod that acts as both a neutron absorber and a heat pipe under accident conditions. The hybrid heat pipe can provide an additional heat transfer path to remove residual heat from the monolith core. It accomplishes this not only by solid-state conduction and radiation but also by phase change heat transfer, while maintaining the compact design of the microreactor. In this study, we designed and conducted experiments on a hybrid cesium heat pipe to investigate its feasibility and thermal behavior through the unique internal structure. The proposed conclusions are as follows:

(1) The hybrid heat pipe established continuum flow at a temperature as low as 205.1°C, allowing for faster startup compared to sodium heat pipes. Experimental startup tests conducted on the cesium hybrid heat pipe confirm its feasibility, particularly at low heat input.

(2) The thermal characteristics of the hybrid heat pipe showed a pronounced converging–diverging effect, with significant temperature gradients within the evaporator and little recovery at the condenser. The temperature drop in the evaporator ranged from 70 to 170°C depending on the heat input, but when entering the condenser, there was a small temperature recovery below 50°C.

(3) In this study, a theoretical analysis of the force–momentum balance was performed to evaluate the effect of changing the flow area of the heat pipe. The results showed that the unique geometry of the hybrid heat pipe has a significant impact on the small pressure recovery at the condenser. Because of the small back pressure, the distinct temperature gradient appeared at the hybrid heat pipe even in the steady state.

(4) Despite the increased prominence of the converging–diverging effect in the hybrid heat pipe, the cesium vapor pressure remains sufficiently high to prevent high velocity, and the condenser operates under natural convection to avoid choked flow. This demonstrates the successful operation of liquid cesium as the working fluid of the heat pipe, overcoming structural limitations.

(5) This study evaluated the performance of a scaled-down hybrid heat pipe for potential use in a microreactor. The heat transfer rate results compared to the operating limit model showed that the partial drying point could be predicted with an error of up to 28.3%. Despite the structural differences, the results showed that the operating limit model can be

used to design the hybrid heat pipe. This is because the hybrid heat pipe design has a large effect on the vapor flow but not on the liquid transport.

This paper demonstrates the feasibility of hybrid heat pipes and shows that the operating limit model can be used to design hybrid heat pipes. It means that the operating limit model can be used to optimize the diameter, length, and wick structure of hybrid heat pipes for microreactor applications. In the future, we will optimize the hybrid heat pipe to the actual microreactor scale based on operating limit models and perform a comprehensive thermal–mechanical analysis of the monolith core with/without the hybrid heat pipe.

## Nomenclature

$M$: Merit number
$P$: Pressure (Pa)
$h_{fg}$: Latent heat of vaporization (kJ/kg)
$Q$: Power (W)
$D$: Diameter (m)
$x_i$: Axial position (−) ($i$ = 1–8)
$T$: Temperature (K)
$h$: Heat transfer coefficient (W/m$^2$ K)
$Kn$: Knudsen number (−)
$R$: Thermal resistance (K/W)
$k$: Thermal conductivity (W/m K)
$L$: Axial length (m)
$A$: Area (m$^2$)
$v$: Velocity (m/s)
$M$: Mach number (−)
$F$: Friction function
$\dot{m}$: Mass flow rate (kg/m s)
Re: Reynolds number (−)
$r$: Radius (m)

### *Greek Symbols*

$\rho$: Density (kg/m$^3$)
$\sigma$: Surface tension (N/m)
$\mu$: Dynamic viscosity (Pa s)
$\varepsilon$: Emissivity (−)
$\Delta$: Differential (−)
$f$: Friction coefficient
$\gamma$: Ratio of specific heat (−)

### *Subscripts*

tr: Transition
$l$: Liquid
$v$: Vapor
eff: Effective
$i$: Inner wall
$o$: Outer wall
rad: Radiation
con: Convection
sat: Saturation
av: Average.

## Data Availability

Data will be available upon request.

## Conflicts of Interest

The authors declare that they have no conflicts of interest.

## Acknowledgments

This work was partly supported by the National Research Foundation of Korea (NRF) grant funded by the Korea Government (MSIT) (no. 2021M2D2A1A03048950) and Korea Institute of Energy Technology Evaluation and Planning (KETEP) grant funded by the Korea Government (MOTIE) (no. RS-2024-00403194, Next-Generation Nuclear Technology Creation IP-R&D Talent (Human Resources) Development Project).

## References

[1] D. Beard, C. Tarau, and W. G. Anderson, "Sodium heat pipes for space and surface fission power," in *15th International Energy Conversion Engineering Conference*, American Institute of Aeronautics and Astronautics, Reston, Virginia, 2017.
[2] J. W. Sterbentz, J. E. Werner, M. G. Mckellar et al., "Special purpose nuclear reactor (5 MW) for reliable power at remote sites assessment report using phenomena identification and ranking tables (PIRTs)," 2017, http://www.inl.gov.
[3] M. M. Swartz, W. A. Byers, J. Lojek, and R. Blunt, "Westinghouse eVinci™ heat pipe micro reactor technology development," in *Proceedings of the 2021 28th International Conference on Nuclear Engineering. (ICONE) Volume 1: Operating Plant Challenges, Successes, and Lessons Learned; Nuclear Plant Engineering; Advanced Reactors and Fusion; Small Modular and Micro-Reactors Technologies and Applications*, American Society of Mechanical Engineers, August 2021.
[4] "Part II: final safety analysis report," 2020.
[5] J. W. Sterbentz, J. E. Werner, A. J. Hummel et al., "Preliminary assessment of two alternative core design concepts for the special purpose reactor," 2018, http://www.inl.gov.
[6] ANS Nuclear Cafe, "Study finds major roles for Westinghouse microreactor in Canada," 2021.
[7] B. J. Marsden, M. Haverty, W. Bodel et al., "Dimensional change, irradiation creep and thermal/mechanical property changes in nuclear graphite," *International Materials Reviews*, vol. 61, no. 3, pp. 155–182, 2016.
[8] T. Cutler, H. Trellue, M. Blood et al., "The hypatia experiment: yttrium hydride and highly enriched uranium critical experiment," *Nuclear Technology*, vol. 209, no. sup1, pp. S92–S108, 2023.
[9] S. Terlizzi and V. Labouré, "Asymptotic hydrogen redistribution analysis in yttrium-hydride-moderated heat-pipe-cooled microreactors using DireWolf," *Annals of Nuclear Energy*, vol. 186, Article ID 109735, 2023.
[10] A. P. Shivprasad, T. E. Cutler, J. K. Jewell et al., "Advanced moderator material handbook," 2020.
[11] S. Qin, M. Song, J. Soo Yoo, P. Sabharwall, and C. M. Petrie, "Code-to-code benchmark study for thermal stress modeling and preliminary analysis of the high-temperature single heat pipe experiment," in *The 19th International Topical Meeting on Nuclear Reactor Thermal Hydraulics (NURETH-19)*, Brussels, Belgium, United States, March 2022.

[12] M. Jeong, *Thermal-Structural Analysis of Micro Reactor Core Using Coupled OpenFOAM and Heat Pipe Code OpenFOAM*, Seoul National University, 2021.
[13] M. J. Jeong, J. Im, S. Lee, and H. K. Cho, "Multiphysics analysis of heat pipe cooled microreactor core with adjusted heat sink temperature for thermal stress reduction using OpenFOAM coupled with neutronics and heat pipe code," *Frontiers in Energy Research*, vol. 11, Article ID 1213000, 2023.
[14] H. C. Hyer, D. C. Sweeney, and C. M. Petrie, "Functional fiber-optic sensors embedded in stainless steel components using ultrasonic additive manufacturing for distributed temperature and strain measurements," *Additive Manufacturing*, vol. 52, Article ID 102681, 2022.
[15] A. Birri, D. C. Sweeney, H. C. Hyer, and C. M. Petrie, "Status update on the development of transducers and bonding techniques for enabling acoustic measurements of damage in microreactor components," 2022, https://www.osti.gov/.
[16] Y. Zhou, J. Wang, Z. Guo et al., "3D-2D coupling multi-dimension simulation for the heat pipe micro-reactor by MOOSE&SAM," *Progress in Nuclear Energy*, vol. 138, Article ID 103790, 2021.
[17] C. Matthews, V. Laboure, M. DeHart et al., "Coupled multiphysics simulations of heat pipe microreactors using DireWolf," *Nuclear Technology*, vol. 207, no. 7, pp. 1142–1162, 2021.
[18] F. Antonello, J. Buongiorno, and E. Zio, "Insights in the safety analysis of an early microreactor design," *Nuclear Engineering and Design*, vol. 404, Article ID 112203, 2023.
[19] Y. S. Jeong, K. M. Kim, I. G. Kim, and I. C. Bang, "Hybrid heat pipe based passive in-core cooling system for advanced nuclear power plant," *Applied Thermal Engineering*, vol. 90, pp. 609–618, 2015.
[20] Y. S. Jeong and I. C. Bang, "Hybrid heat pipe based passive cooling device for spent nuclear fuel dry storage cask," *Applied Thermal Engineering*, vol. 96, pp. 277–285, 2016.
[21] I. G. Kim and I. C. Bang, "Spent nuclear fuel with a hybrid heat pipe for electricity generation and thermal management," *Energy Conversion and Management*, vol. 173, pp. 233–243, 2018.
[22] L. M. Alawneh, R. Vaghetto, Y. Hassan, and H. G."Sonny" White, "Conceptual design of a 3 MWth yttrium hydride moderated heat pipe cooled micro reactor," *Nuclear Engineering and Design*, vol. 397, Article ID 111931, 2022.
[23] N. Stauff, C. Lee, and C. Filippone, "Core design of the holos-quad microreactor," Argonne National Laboratory (ANL), Argonne, IL (United States), Tech. Rep, 2022.
[24] P. D. Dunn and D. A. Reay, "The heat pipe," *Physics in Technology*, vol. 4, no. 3, pp. 187–201, 1973.
[25] P. M. Dussinger, W. G. Anderson, and E. T. Sunada, "Design and testing of titanium/cesium and titanium/potassium heat pipes," in *Proceedings of the 2005 IECEC*, pp. 15–18, AIAA, 2005.
[26] D. Lee and I. Bang, "Investigation of hybrid heat pipe shutdown rod concept of microreactor as a passive safety system," in *20th International Topical Meeting on Nuclear Reactor Thermal Hydraulics (NURETH-20)*, pp. 3456–3467, American Nuclear Society, Illinois, August 2023.
[27] J. E. Kemme, "Ultimate heat-pipe performance," *IEEE Transactions on Electron Devices*, vol. 16, no. 8, pp. 717–723, 1969.
[28] H.-X. Chen, Y.-X. Guo, D.-Z. Yuan, and Y. Ji, "Experimental study on frozen startup and heat transfer characteristics of a cesium heat pipe under horizontal state," *International Journal of Heat and Mass Transfer*, vol. 183, Article ID 122105, 2022.
[29] S. W. Churchill and H. H. S. Chu, "Correlating equations for laminar and turbulent free convection from a vertical plate," *International Journal of Heat and Mass Transfer*, vol. 18, no. 11, pp. 1323–1329, 1975.
[30] K. M. Kim and I. C. Bang, "Thermal-hydraulic phenomena inside hybrid heat pipe-control rod for passive heat removal," *International Journal of Heat and Mass Transfer*, vol. 119, pp. 472–483, 2018.
[31] C. Mueller and P. Tsvetkov, "Novel design integration for advanced nuclear heat-pipe systems," *Annals of Nuclear Energy*, vol. 141, Article ID 107324, 2020.
[32] A. Faghri, *Heat Pipe Science and Technology*, Global Digital Press, 1995.
[33] J. E. Deverall, J. E. Kemme, and L. W. Florschuetz, "Sonic limitations and startup problems of heat pipes. No. LA-4518," Los Alamos National Lab. (LANL), Los Alamos, NM (United States), Tech. Rep, 1970.
[34] C. Wang, X. Liu, M. Liu et al., "Experimental study on heat transfer limit of high temperature potassium heat pipe for advanced reactors," *Annals of Nuclear Energy*, vol. 151, Article ID 107935, 2021.
[35] M. N. Ivanovskii, V. V. Prosvetov, V. P. Sorokin, B. A. Chulkov, and I. V. Yagodkin, "Investigation of the evaporation process and sonic limits in sodium heat pipes," *Journal of Engineering Physics*, vol. 33, no. 5, pp. 1306–1310, 1977.
[36] Z. Tian, J. Zhang, C. Wang et al., "Experimental evaluation on heat transfer limits of sodium heat pipe with screen mesh for nuclear reactor system," *Applied Thermal Engineering*, vol. 209, Article ID 118296, 2022.
[37] M. Zhang, Q. Miao, S. Zhang et al., "Experimental study of non-condensable gas effects on sonic limit of sodium heat pipe," *Applied Thermal Engineering*, vol. 232, Article ID 120970, 2023.
[38] I. Yilgor and S. Shi, "Scaling laws for two-phase flow and heat transfer in high-temperature heat pipes," *International Journal of Heat and Mass Transfer*, vol. 189, Article ID 122688, 2022.
[39] H.-X. Chen, Y.-X. Guo, D.-Z. Yuan, and Y. Ji, "Thermal performance of a medium temperature cesium heat pipe at different inclination angles," *International Communications in Heat and Mass Transfer*, vol. 138, Article ID 106363, 2022.
[40] E. K. Levy and S. F. Chou, "The sonic limit in sodium heat pipes," *Journal of Heat Transfer*, vol. 95, no. 2, pp. 218–223, 1973.
[41] S. W. Chi, "Heat pipe theory and practice: a sourcebook," 1976.